TSR TRAFFIC SAFETY RESEARCH
AN INTERDISCIPLINARY JOURNAL

Kumar, R. S., & Kumar, V. R. (2026). A data-driven framework for assessing horizontal curve safety using friction and reliability analysis: a case study on an Indian highway. *Traffic Safety Research*, *10*, e000139. https://doi.org/10.55329/uzno7733

Research article

A data-driven framework for assessing horizontal curve safety using friction and reliability analysis: a case study on an Indian highway

R. Srinivasa Kumar[1,a], Vemula Rajesh Kumar[1]

[1]Osmania University, India

Keywords: safety index, reliability analysis, global sensitivity, advisory speed prediction

https://doi.org/10.55329/uzno7733

Horizontal curves are frequently associated with elevated crash risk because of the combined effects of vehicle speed, roadway geometry, and tire–pavement friction. This study examines these interactions using field data collected from five horizontal curves on NH-340C in India. An empirical model for estimating the maximum available side friction was developed using measured vehicle speeds, superelevation, and pavement surface texture represented by Mean Texture Depth (MTD). Curve safety was evaluated using three complementary indicators: the Safety Index (SI), Change in Safety Index (ΔSI), and Dynamic Curve Safety Index (DCSI), which together describe local stability conditions and safety variations along the curve. The calibrated friction model shows a decrease in available friction with increasing speed and a moderate increase with pavement texture, producing values in the range of 0.16–0.28 that are consistent with international design guidelines. Model reliability was evaluated using uncertainty and sensitivity analysis techniques, including the delta method, bootstrap resampling, the First-Order Reliability Method, and global sensitivity analysis using Sobol and Morris approaches. The results indicate that pavement texture and operating speed are the dominant factors influencing friction variability, while superelevation has a comparatively smaller effect. In addition, a regression-based model was developed to estimate mid-curve operating speeds, which can support the determination of advisory speeds for curve safety management.

1. Introduction

Road safety is a global public health priority, as motorization and travel demand continue to rise faster than improvements in infrastructure and enforcement (WHO, 2023). Horizontal curves are consistently identified as high-risk roadway elements because they require drivers to adjust speed, maintain steering precision, and adapt to varying tire-pavement friction. Failures in these tasks, particularly under low-friction conditions, are a major cause of loss-of-control crashes (AASHTO, 2018; Donnell et al., 2016). Although curves represent only a small share of road length, they account for 20–30% of severe crashes, often intensified by excessive speed, inadequate superelevation, surface deterioration, and insufficient friction (Shalkamy et al., 2021).

India continues to face a severe road safety challenge. In the year 2022, 461,312 crashes caused 168,491 deaths and 443,366 injuries, equivalent to 53 crashes and 19 deaths every hour, with year-on-year increases of 11.9%, 9.4%, and 15.3% (MoRTH, 2022, 2023, 2024). Curve-related crashes alone accounted for 54,593 incidents and 20,573 deaths, while overturning crashes added 20,070 incidents

[a] Corresponding author: rungoz@osmania.ac.in

and 9,829 deaths (MoRTH, 2022). Field records from NH-340C further highlight this risk on five study curves experienced 22 crashes and 12 fatalities between 2020 and May 2025. The Krishnapuram Anjineya Swamy Statue curve recorded nine crashes and three deaths due to rash manoeuvres, while Venkatapuram, despite only three crashes, caused eight fatalities linked to over-speeding and animal crossings. These observations underscore the urgent need for localized safety diagnosis and targeted interventions.

Key contributing factors in India include heterogeneous traffic ranging from two-wheelers to heavy trucks, rapid pavement deterioration due to monsoons and poor drainage, mismatches between design and operating speeds, and risky behaviours such as late braking and curve-overtaking (Singh, 2017; Dash et al., 2020; Shailaja et al., 2022; Rosas-López et al., 2021). Among curve types, simple circular curves pose higher risks than spirals because lateral forces depend heavily on speed, radius, superelevation, and pavement condition (Chen et al., 2007, Sharf Aldeen et al., 2022).

Safe negotiation of curves depends on balancing the demand and supply of side friction. The maximum side friction factor (F_{max}) reflects available supply and is shaped by pavement texture, materials, climate, and tire properties (McLean, 1981; AASHTO, 2018; Gattis et al., 2005; Abohassan et al., 2022). Current Indian standards (IRC, 2023) assume a fixed F_{max} of 0.15 regardless of speed, texture, or traffic heterogeneity, risking both under- and over-design (Nicholson, 1998; Morrall & Talarico, 1994). Research has consistently shown friction to be speed-dependent. Barnett (1938) recommended reductions beyond 60 mph, McLean (1981) linked failures to inadequate superelevation, and Mudry (1999) demonstrated that 85th percentile friction often exceeded AASHTO limits (Shalkamy et al., 2021). Bonneson (1999, 2000) confirmed higher friction acceptance at lower speeds and suggested using the 95th percentile of speeds for design, while Fitzpatrick et al. (2000) showed that stability is most compromised at midpoints. These findings stand against static assumptions and call for dynamic speed–friction models in safety evaluation.

Speed profiling has been widely used to study driver behavior, consistently showing deceleration before entry, minimum speed at midpoints, and acceleration at exits. These trends are influenced by curve radius, superelevation, sight distance, shoulder provision, and approach speed (Bennett, 1994; Gong & Stamatiadis, 2008; Bonneson & Pratt, 2009; Shallam & Ahmed, 2016; Llopis-Castelló et al., 2018). Extended deceleration zones often cause discomfort and instability, particularly on circular compared with spiral curves (Chen et al., 2007; Montella & Imbriani, 2015; Himes et al., 2019; Han et al., 2023). Approach speed strongly governs mid- and exit speeds, which in turn influence vehicle stability and crash risk (Himes et al., 2019). Previous models have attempted to predict operating speeds using geometric variables such as shoulder width, radius, superelevation, and sight distance (Bennett, 1994; Gong & Stamatiadis, 2008; Bonneson & Pratt, 2009; Shallam & Ahmed, 2016; Semeida, 2014; Llopis-Castelló et al., 2018). Others stressed the role of approach speed in enabling timely driver alerts, since long deceleration zones reduce comfort and safety (Montella & Imbriani, 2015).

With advances in data-driven approaches, machine learning has been increasingly applied in transportation safety. Applications include lane-change prediction (Zhao et al., 2022), traffic speed forecasting with SHAP explanations (Lee, 2023), crash detection from speed analysis (Parsa et al., 2020), freeway crash prediction using Bayesian networks and XGBoost (Yang et al., 2022), real-time cab speed estimation (Shen, 2022), travel time prediction (Chen & Fan, 2021), and high-speed urban traffic flow modelling (Lu et al., 2023). However, limited research has focused on predicting reliable operating speeds at approach, midpoint, and exit sections of horizontal curves under mixed-traffic and pavement conditions. This gap highlights the need for models that integrate speed–friction dynamics with local roadway and behavioural factors.

Advisory speed plaques remain a standard tool for curve safety management (Traffic, 2009). Research has linked advisory speeds to crash–radius relationships (Bonneson et al., 2007; Fitzpatrick et al., 2000; Milstead et al., 2011; Montella & Imbriani, 2015) and factors such as speed differentials (Figueroa Medina & Tarko, 2007; Pratt et al., 2015), curve geometry (Dixon & Rohani, 2008), side friction (Dixon & Rohani, 2008), superelevation (Bonneson & Pratt, 2009; Pratt et al., 2019), and signage (Hummer et al., 2010). However, static advisory speeds are often ineffective because of design inconsistencies (Nicholson, 1998), variable driver behaviour (Fleiter & Watson, 2005), attitudes (Hassen et al., 2011), and decision-making patterns (Warner & Åberg, 2006). Recent advances favour adaptive systems that continuously monitor vehicles and deliver dynamic feedback. Customized techniques create adjustable alerts (Davis et al., 2018), while automated systems provide real-time visual or audio warnings when drivers approach curves at unsafe speeds (Davis et al., 2018; Mahmud et al., 2023).

Despite international research, little work has focused on developing field-based friction models or adaptive speed frameworks for Indian highways, where mixed traffic, heterogeneous driving behaviour, and pavement surface texture variability exacerbate safety risks. To address this gap, the present study pursues four objectives:

1. Develop an India-specific maximum side friction function dependent on speed, texture, and superelevation, calibrated against AASHTO envelopes.
2. Address the need for field-based $F^*_{\max}$ modelling under Indian traffic and validating by uncertainty analysis.
3. Evaluate curve safety using three indices: Safety Index (SI), Change in Safety Index (ΔSI), and Dynamic Curve Safety Index (DCSI).
4. Predict mid-curve operating speeds through regression, with advisory speeds suggested for real-time alerts via adaptive signage.

By integrating a calibrated $F^*_{\max}$ model, SI-based diagnostics, and detailed speed profiles, this study offers a data-driven framework for identifying hazardous curves and guiding India-specific design standards, safety audits, and real-time risk management strategies (Montella & Imbriani, 2015; Abohassan et al., 2022).

2. Methodology

This study develops a framework for evaluating horizontal curve safety under Indian roadway conditions through four steps: (i) field data collection, (ii) development of a locally calibrated maximum side friction model ($F^*_{\max}$), (iii) safety index evaluation, and (iv) mid-curve speed prediction for real-time warnings.

Field surveys recorded curve geometry (radius, superelevation) and operating speeds (tangent, entry, middle, and exit) as well as pavement texture (Mean Texture Depth, MTD, via the sand patch method). These inputs were used to develop a nonlinear empirical model of $F_{\max}$, expressed as $F^*_{\max} = a * MTD^b * Speed^{-c} * e^d$, where parameters *a, b, c,* and *d* were calibrated against AASHTO (2018) values using nonlinear regression to capture Indian conditions. The calibrated F_{max} values were compared with the side friction demand:

$$F_d = \frac{V^2}{g.R} - e \tag{1}$$

The actual side friction demand values were quantified for safety assessment using three indices: the Safety Index (SI), Change in Safety Index (ΔSI), and Dynamic Curve Safety Index (DCSI). These indices enabled a systematic assessment of how safety varies from curve entry to exit. Subsequently, mid-curve operating speeds identified as critical for stability were predicted using a regression model, based on geometric and field data. This model generated advisory speed values derived from SI, supporting proactive warnings through adaptive roadside signs or in-vehicle systems.

The analytical framework integrates deterministic modelling, uncertainty

quantification, and safety diagnostics. The nonlinear regression establishes the friction model, while the delta method and bootstrap quantify parameter uncertainty. First-Order Reliability Method (FORM) translates these uncertainties into reliability-based safety probabilities, and global sensitivity analysis identifies dominant influencing variables.

3. Study sites and data collection

Five horizontal curves were selected on National Highway 340C (NH-340C) in Andhra Pradesh for detailed investigation, considering their accident history and geometric complexity. The study curves represent a broad range of radii, superelevation levels, pavement texture conditions, and crash histories commonly observed on rural two-lane highways in India. The selected sites include the Pamulapadu curve, Banumukula curve, Krishnapuram statue curve, Krishnapuram curve, and Venkatapuram curve. For each location, geometric characteristics such as chainage, radius, superelevation, roadway width, and deflection angle were surveyed to serve as input variables for the development of side friction and safety models. The radii of the selected curves ranged from 50 m to 180 m, while superelevation varied between 4.0% and 7.0%, and carriageway widths were consistently about 7.0–7.2 m. Although the curves were designed for a nominal speed of 80 km/h, field observations revealed notable deviations in actual operating speeds.

All geometric, traffic, pavement texture, and speed data were collected separately for each individual curve location. Independent field surveys were conducted at each site to capture roadway-specific operating characteristics, pavement conditions, and traffic behavior under mixed-traffic conditions.

Figure 1 presents the geographical location of the five selected study curves along NH-340C in Andhra Pradesh, India. The map illustrates the spatial distribution of the investigated sites between Pamulapadu and Venkatapuram.

The field investigations comprised measurements of spot speeds at tangent (pre-start), entry, middle, and exit locations; derivation of acceleration–deceleration profiles; measurement of Mean Texture Depth (MTD) using the sand-patch method; and detailed surveying of curve geometry. The MTD values at curve midpoints ranged from 0.380 mm to 1.123 mm, reflecting pavement surface variability. Table 1 summarizes the geometric parameters and surface conditions of the study curves.

3.1 Traffic survey procedure

In addition to geometry, traffic flow data were collected to assess exposure risk. Traffic flow and speed surveys were conducted during multiple field campaigns between January 2024 and May 2025 under representative traffic conditions. Classified traffic volume counts were conducted at representative sections along the study corridor using manual observations supported by video recording for verification. The observed traffic volumes were converted into Passenger Car Units (PCU/day) using IRC (2023) recommended equivalency factors for heterogeneous traffic streams. The annual average daily traffic was estimated at 3,975 passenger car units per day, with a peak hour factor of 0.74, indicating marked variations between peak and off-peak periods. The traffic stream was dominated by two-wheelers (50.7%), followed by three-wheelers (15.0%) and cars/jeeps (14.3%). Heavy vehicles contributed smaller proportions, including light commercial vehicles (9.4%), buses (5.1%), trucks (4.1%), and non-motorized vehicles (1.4%).

To investigate vehicle operating behaviour under mixed traffic-flow conditions, spot speed surveys were conducted along the five selected horizontal curves on NH-340C during multiple field campaigns between January 2024 and May 2025. Surveys were performed during daylight hours under dry pavement conditions to minimize the influence of rainfall, poor visibility, and wet-surface friction variations. Observations were collected during representative morning, mid-

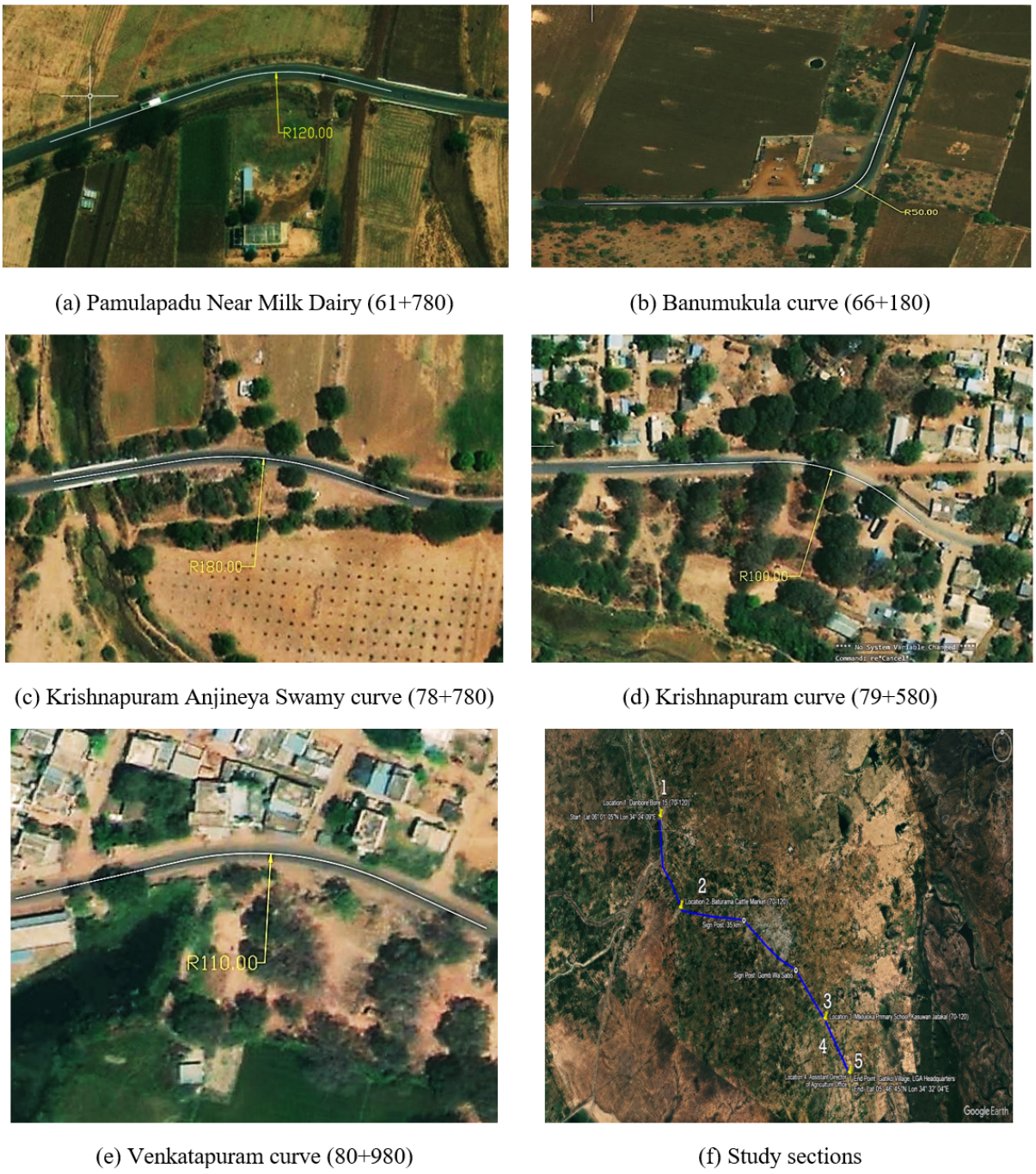

(a) Pamulapadu Near Milk Dairy (61+780)

(b) Banumukula curve (66+180)

(c) Krishnapuram Anjineya Swamy curve (78+780)

(d) Krishnapuram curve (79+580)

(e) Venkatapuram curve (80+980)

(f) Study sections

Figure 1. Geographical location and representative field photographs of the selected study curves along NH-340C in Andhra Pradesh, India

day, and evening periods under free-flow traffic conditions while avoiding abnormal situations such as severe congestion, maintenance activity, or traffic diversions. High-precision radar speed guns were used to record spot speeds at four locations along each curve at, tangent (pre-start), entry, midpoint, and exit sections. The collected data covered major vehicle categories including two-wheelers, three-wheelers, cars, buses, and trucks. Each survey session continued until stable speed distributions were obtained for all vehicle classes.

The speed profiles (Figure 2) indicate a consistent trend of deceleration from Pre-Start to the Middle of the curve, followed by partial recovery toward the Exit. Cars

Table 1. Geometric parameters of the five study curves on NH-340C

Curve #	*#1*	*#2*	*#3*	*#4*	*#5*
Location	Pamulapadu near Milk Dairy	Banumukula curve	Krishnapuram Anjineya Swamy curve	Krishnapuram curve	Venkatapuram curve
KM Post	61+780	66+180	78+780	79+580	80+980
Coordinates	15°50'32.64"N 78°29'57.78"E	15°49'57.12"N 78°32'32.56"E	15°52'58.51"N 78°38'9.76"E	15°52'58.57"N 78°38'34.60"E	15°53'0.41"N 78°39'21.29"E
Radius (m)	120	50	180	100	110
Superelevation (%)	5.0	7.0	4.0	5.0	5.0
Carriageway width (m)	7.20	7.10	7.00	7.10	7.20
Design speed (Kmph)	80	80	80	80	80
R1 -Inner radius(m)	118.20	48.25	178.25	98.25	108.20
R2 - outer radius (m)	121.80	51.75	181.75	101.75	111.80
Deflection Angle (Δ_1)	12 30'	50° 58′ 27″	26° 31′ 00″	15° 01′ 00″	14° 47′ 00″
Deflection Angle (Δ_2)	12 30'	50° 00′ 44″	26° 31′ 00″	16° 09′ 00″	14° 48′ 00″
MTD_{middle} Average (mm)	0.391	0.993	0.570	1.123	0.380

exhibited the highest operating speeds across all sections, with average speeds of 79.1 km/h at the tangent and 61.4 km/h at the curve midpoint, whereas three-wheelers recorded the lowest midpoint speeds (24.6 km/h). Standard deviation analyses revealed greater heterogeneity in car speeds (16.9–18.0 km/h) compared to the more uniform speeds of three-wheelers (7.6–8.4 km/h). Maximum speed observations reinforced these differences, with cars reaching up to 119 km/h at tangents while three-wheelers rarely exceeded 38 km/h at the curve midpoint. These results demonstrate that vehicle type and maneuverability strongly influence curve negotiation behavior in mixed traffic-flow conditions.

Analysis of longitudinal dynamics highlighted distinct behavioral phases: sharp deceleration during curve entry (up to –6.3 m/s^2 for cars), sustained negative acceleration through the curve midpoint (–0.8 to –1.3 m/s^2 across vehicle types), and mild positive acceleration during exit (+0.5 to +1.2 m/s^2). Although drivers attempted to regain speed at the exit, recovery seldom matched tangent speeds, emphasizing the restrictive influence of horizontal curvature. The consistent patterns across vehicle types, coupled with variation in acceleration magnitudes, reflect differences in stability, driver response, and traffic heterogeneity.

The observed speed patterns, characterized by cautious entry speeds, controlled mid-curve travel, and partial exit recovery, reflect adaptive driver behavior under friction constraints. Repeated deceleration and limited speed recovery highlight potential instability when demand friction nears availability, reinforcing the necessity of safety indices to quantitatively relate driver response to curve geometry in mixed traffic environments.

4. Development of F^*_{max} for Indian conditions

A maximum side friction factor ($F^*_{\max}$) model for Indian conditions was developed using field-measured parameters, including Mean Texture Depth (MTD), midpoint operating speed, and superelevation (e). These inputs were analyzed using a nonlinear regression framework to ensure that the resulting model realistically captures pavement–tire interactions and mixed-traffic dynamics.

The general model structure was specified as:

$$F^*_{\max} = a * MTD^b * Speed^{-c} * e^d \quad (2)$$

where constants *a, b, c,* and *d* were estimated through optimization.

For each observation *i*, the model prediction is:

$$\widehat{F}_{\max,i}(a,b,c,d) = a \times MTD_i^b \times Speed_i^{-c} \times e_i^d \quad (3)$$

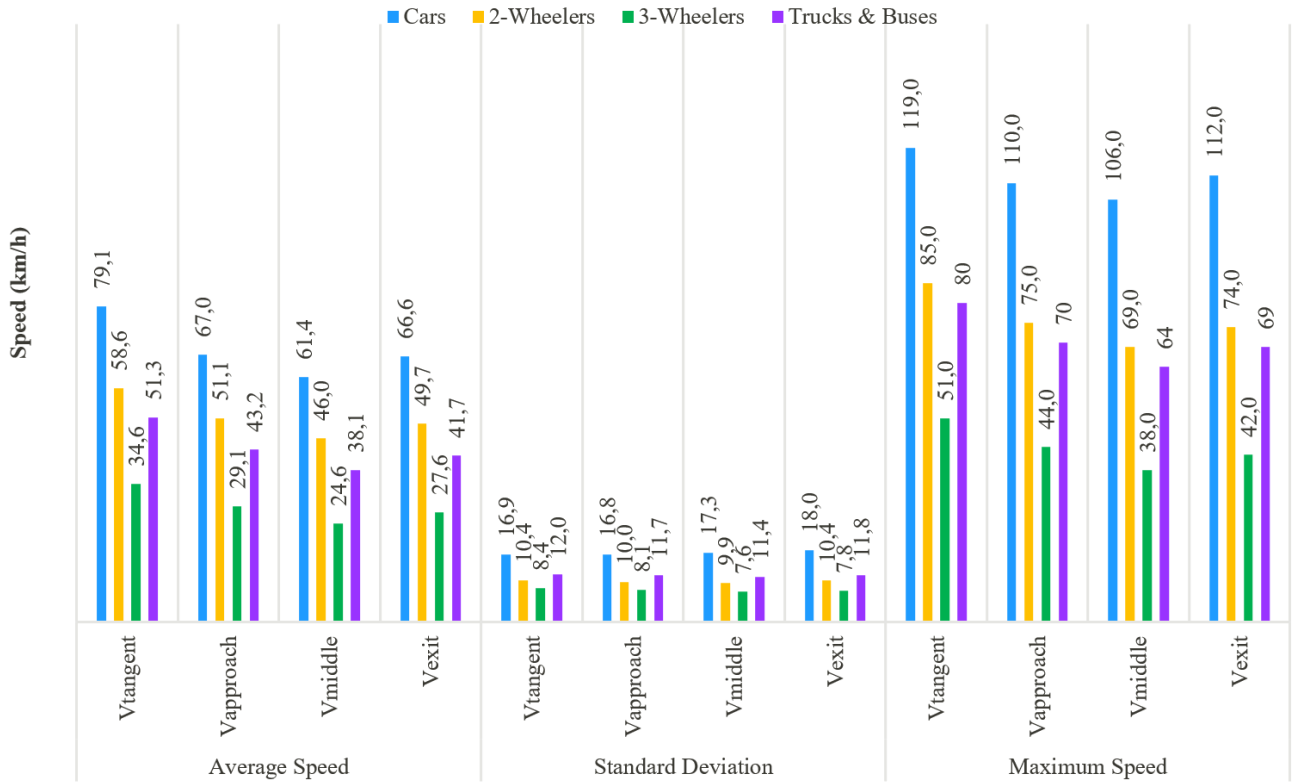

Figure 2. The speed profiles of vehicles travelling on circular horizontal curves

Residual at row i (what the optimizer tries to drive toward zero):

$$r_i(a,b,c,d) = F_{max,i}^{(AASHTO)} - \widehat{F}_{\max,i}(a,b,c,d) \quad (4)$$

Stacking residuals into a vector $r(\Theta) \in \mathbb{R}^n$, the objective minimized is the sum of squared errors (SSE):

$$SSE(\Theta) = \sum_{i=1}^{n} r_i(\Theta)^2 \quad (5)$$

Conceptually, (Virtanen et al., 2020) start from an initial guess $\Theta^{(0)}$. Later, Updates and to reduce SSE using a Gauss-Newton-type step with damping (Levenberg-Marquardt) or a trust-region method when bounds are used (Levenberg, 1944; Marquardt, 1963). Finally, stops when the gradient is small or the maximum number of iterations is reached. When no bounds are imposed, *SciPy* historically uses a Levenberg-Marquardt approach for performing nonlinear least-squares minimization (More et al., 1980). It uses the Jacobian to numerically approximate curvature (via finite differences) and take curvature-aware steps by solving (Moré, 1978; Virtanen et al., 2020).

$$(J^T \cdot J + \lambda I)\Delta_p = J^T \cdot r \quad (6)$$

where J is the Jacobian of residuals and λ is the damping; J^T: Transpose of the Jacobian; I: Identity matrix, Δp: Parameter update vector. Added to the current parameter vector in each iteration:

$$p_{new} = p_{current} + \Delta_p \quad (7)$$

Residual vector = $r_i = y_i - f(x_i;p)$

For each residual r_i, the solver uses sensitivities $\partial r_i/\partial a$, $\partial r_i/\partial b$, $\partial r_i/\partial c$, $\partial r_i/\partial d$, which for the model follow from and *SciPy* approximates these numerically.

$$\widehat{F}_{\max,i=a.\ X_i,} \qquad X_i = MTD_i^b.Speed_i^{-c}.e_i^d \quad (8)$$

Hence,

$$\frac{\partial \widehat{F}_{\max,i}}{\partial a} = X_i, \frac{\partial \widehat{F}_{\max,i}}{\partial B} = aX_i \ln(MTD)_i,$$

$$\frac{\partial \widehat{F}_{\max,i}}{\partial c} = a\ X_i \ln(speed),$$

$$\frac{\partial \widehat{F}_{\max,i}}{\partial B} = aX_i \ln(e_i)$$

differences. Conceptually, it is expected that *b* > *0* (greater texture yields more friction), *c* > *0* (larger *c* indicates stronger reduction of friction with increasing speed), and *d* may be small but positive (superelevation marginally enhances available friction). Also, takes a > 0.

To improve numerical stability, a log-linear transformation was applied for initial parameter estimation:

$$\ln F^*_{\max} = \ln a + b, \\ \ln(MTD) - c \cdot \ln(Speed) + d \cdot \ln(e) \quad (9)$$

Let, $y = \ln F_{\max}$, $x_1 = \ln MTD$, $x_2 = \ln Speed$, $x_3 = \ln e$

Runs an ordinary least squares on $y = \beta 0 + \cdot x_1 + \beta 2 \cdot (-x_2) + \beta 3 \cdot x_3$

Ordinary least squares on this linearized form provided initial guesses and set: $a^{(O)} = e^{\beta_0}$, $b^{(0)} = \beta_1$, $c^{(0)} = -\beta_2$, $d^{(0)} = \beta_3$

These values were supplied to the nonlinear solver to accelerate convergence. The parameter vector was optimized as:

$$\left(\widehat{\theta}, \widehat{\sum}\right) = \textbf{curve\_fit(f,X,y)with } \widehat{\theta} = (\widehat{a}, \widehat{b}, \widehat{c}, \widehat{d}) \quad (10)$$

Where, $\widehat{\theta}$ are the best-fit parameters that minimize the sum of squared errors (SSE), $\widehat{\sum}$ is the estimated covariance matrix derived from the Jacobian at the solution. From this, the standard error for parameter k was obtained as:

$$SE\left(\widehat{\Theta}_k\right) = \sqrt{\widehat{\sum}_{kk}} \quad (11)$$

And the 95% confidence intervals were computed as,

$$\widehat{\Theta}_k \pm 1.96\, SE(\widehat{\Theta}_k) \quad (12)$$

The above ensures the statistical reliability of the fitted parameters. The calibrated Indian-specific predictive model was obtained as:

$$F^*_{\max} = 1.5721 * MTD^{-0.5508} \\ * Speed^{-0.583} * e^{0.033} \quad (13)$$

This functional form captures the nonlinear influence of pavement surface texture, speed, and geometry on the tire-road interaction. Predicted values ranged between 0.16 and 0.28, closely matching the AASHTO reference range of 0.15–0.30 while explicitly capturing Indian roadway conditions.

5. Uncertainty analysis

The uncertainty in $F^*_{\max}$ is evaluated by the following methods.

5.1 Delta-method variance estimation

Uncertainty in $F^*_{\max}$ due to parameter sensitivity is estimated using the first-order delta method and estimated through the propagation of parameter uncertainty (Beutner, 2024). Let Θ = [*a, b, c, d*]^T and the covariance matrix Σ_θ. Then:

$$Var\left[F^*_{\max}\right] \approx \nabla_\theta F^{*T}_{\max} \Sigma_\theta \nabla_\theta F^*_{\max} \quad (14)$$

Where $\nabla_\theta F^*_{\max}$ is the gradient vector with respect to parameters:

$$\nabla_\theta F^*_{\max} = \begin{bmatrix} \frac{\partial F^*_{\max}}{\partial a} \\ \frac{\partial F^*_{\max}}{\partial b} \\ \frac{\partial F^*_{\max}}{\partial c} \\ \frac{\partial F^*_{\max}}{\partial d} \end{bmatrix} = \begin{bmatrix} \frac{F^*_{\max}}{a} \\ F^*_{\max} \ln(MTD) \\ F^*_{\max} \ln(V) \\ F^*_{\max} \ln(e) \end{bmatrix} \quad (15)$$

Assuming independent parameter uncertainties,

$$\Sigma_\theta = diag\left[(0.05a)^2,\ (0.05b)^2, (0.05c)^2, (0.05d)^2\right]$$

A coefficient of variation of 5% was adopted for parameter uncertainty following common practice in transportation reliability analysis, where geometric and pavement measurement errors typically range between 3–7%. This assumption provides a conservative estimate of model variance while avoiding unrealistic uncertainty amplification (Melchers & Beck, 2018)

The standard deviation of $F^*_{\max}$ is:

$$\sigma_F = \sqrt{Var\left[F^*_{\max}\right]} \quad (16)$$

and the 95% confidence bounds are given by:

$$F^*_{max,\ lower} = F^*_{\max} - 1.96\sigma_F, \\ F^*_{max,\ upper} = F^*_{\max} + 1.96\sigma_F \quad (17)$$

Table 2 presents the numerical outcomes of the delta-method uncertainty analysis. These reveal that $F^*_{\max}$ sharply decreases with increasing operating speed, increases moderately with surface texture depth, and is only weakly enhanced by superelevation. The sensitivity magnitudes confirm that pavement texture and speed dominate frictional response, while the geometric term *e* exerts a positive influence.

5.2 Local elasticity analysis

The elasticity of $F^*_{\max}$with respect to each input, its percentage sensitivity (De Kroon et al., 2000):

$$E_{x_i} = \frac{\partial \ln F^*_{\max}}{\partial \ln x_i} \tag{18}$$

Given Eq. (13), the elasticities are considered as:

$E_{MTD} = b = -0.5508$, $E_V = c = -0.583$, $E_e = d = 0.033$

A tornado-style plot (Figure 3) illustrates the relative elasticities of $F^*_{\max}$ with respect to MTD, Speed, and *e*. Speed exhibits the highest negative sensitivity, followed by MTD, confirming its dominant influence on available side friction, whereas *e* contributes comparatively less positive influence.

Bootstrap confidence intervals: To evaluate the statistical robustness of parameters, nonparametric bootstrap resampling is applied to the log-linearized model in Eq. (9). The model was resampled, N_{boot} = 200 times with replacement, refitted in each iteration, and the empirical distribution of the resulting parameter vectors θ_i = (*a, b, c, d*) was used to derive mean estimates and 95 % confidence bounds as (Mokhtar et al., 2023):

$$\theta_i^{(low)},\ \theta_i^{(high)} = Percentile_{(2.5,\ 97.5)}\left[\theta_i^*\right] \tag{19}$$

The results summarized in Table 3 demonstrate narrow confidence ranges for all four parameters, indicating that the nonlinear calibration is statistically stable and not overly sensitive to random sampling variation.

Figure 4 interprets conceptually in the model calibration. It demonstrates the inverse power-law dependency between available friction and speed, confirming that as vehicle speed increases, $F^*_{\max}$ declines exponentially.

5.3 Reliability analysis

Under the First-Order Reliability Method (FORM) framework, the limit-state function separates safe and failure domains as (Zhou et al., 2017):

$$g(V,\ R,\ MTD,\ e) = F^*_{\max}(V,\ R,\ MTD,\ e) - F_d(V,\ R,\ e) \tag{20}$$

Failure occurs when g < 0.

Assuming normal uncertainty in $F^*_{\max}$, and the corresponding reliability index (β) and failure probability (P_f) are derived from the probabilistic relationship

$$\beta = \frac{g}{F_d\,|F^*_{\max}|},\quad P_f = \Phi(-\beta) \tag{21}$$

where $\Phi(\square)$ denotes the cumulative normal distribution function.

Advisory speeds $V_{adv}(\beta)$ are computed for target reliability thresholds (β_t = 0.10,0.05,0.02,0.01) by iteratively solving:

$$P_f\left(V_{adv}\right) = \beta_t \tag{22}$$

The reliability curves plot *P*(*SI*<1) as a function of speed for each vehicle type, and Cars exhibited the highest probability of failure (Figure 4). The intersections of the probability curve with the dashed horizontal lines (β_t) yield the advisory operating speeds (e.g., 22.56–23.16 m/s for the car case). The *FORM-derived reliability surface*, where smaller P_f values correspond to safer operating conditions and higher margins of frictional stability.

5.4 Global sensitivity analysis

To assess overall influence ranges, global variance-based methods are applied to quantify the relative influence of texture (MTD), speed, and superelevation (e) on the predicted $F^*_{\max}$:

Table 2. Delta-Method Variance and Elasticities Summary

Quantity	Symbol	Equation	Typical Value (Mean ± SD)	Interpretation
Predicted friction	$F^*_{\max}$	$1.5721 \times MTD^{-0.5508} \times Speed^{-0.583} \times e^{0.033}$	0.18 ± 0.02	Central model prediction
Variance (Delta)	$Var\,[F^*_{\max}]$	$\nabla_\theta F^{*T}_{\max} \Sigma_\theta \nabla_\theta F^*_{\max}$	1.1×10^{-4}	Parameter-induced variability
Std. deviation	σ_F	$\sqrt{Var\,[F^*_{\max}]}$	0.010–0.020	68 % confidence width
Elasticity wrt MTD	$E_{MTD} = b$	$\frac{\partial \ln F}{\partial \ln MTD}$	−0.5508	Texture moderately increases friction
Elasticity wrt Speed	$E_V = c$	$\frac{\partial \ln F}{\partial \ln V}$	−0.583	Friction decreases strongly with speed
Elasticity wrt e	$E_e = d$	$\frac{\partial \ln F}{\partial \ln e}$	+0.033	Minor geometric contribution

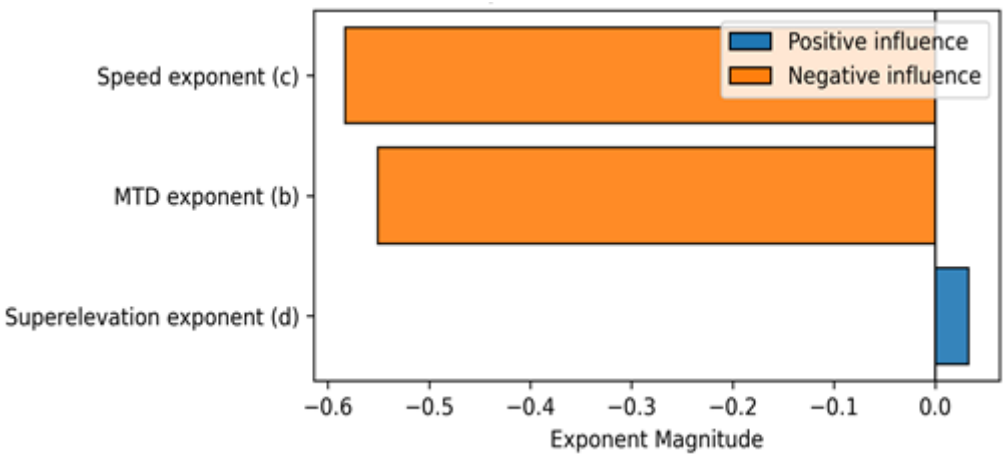

Figure 3. Elasticity tornado plot of $F^*_{\max}$ model

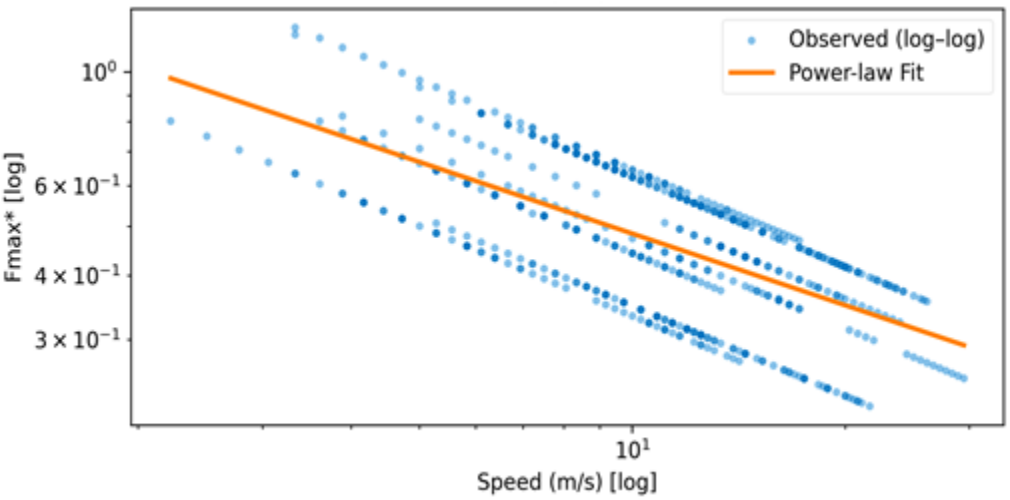

Figure 4. $F^*_{\max}$ vs speed variation

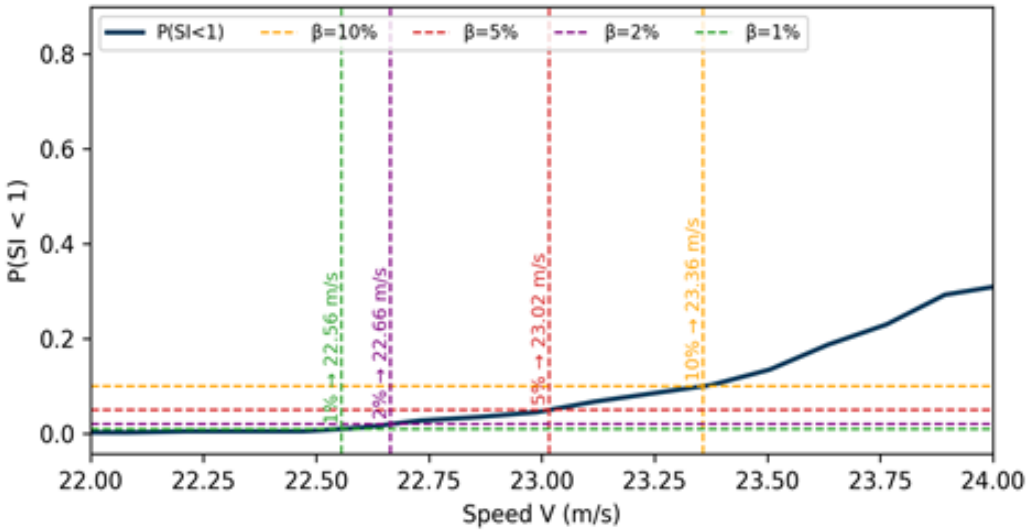

Figure 5. Reliability curve for the car plot of $F^*_{\max}$– speed relationship

Table 3. Confidence Intervals

Parameter (log-linearized)	Mean	Confidence Interval low	Confidence Interval high
Scale coefficient	0.095358	0.02909	0.156274
Texture exponent	0.001336	−0.00682	0.010113
Speed exponent	0.653567	0.638691	0.667525
Superelevation exponent	−0.00083	−0.02038	0.019295

(i) Sobol's indices by Saltelli sampling (Sobol, 2001; Saltelli et al., 2010):

$$S_i = \frac{Var_{X_i}(Y|X_i)}{Var(Y)}, \qquad S_{T_i} = 1 - \frac{Var_{X_{\sim i}}(Y|X_{\sim i})}{Var(Y)} \tag{23}$$

where S_i and S_{T_i} represent first-order and total effects, respectively.

Sobol's indices (Table 4), the global sensitivity indices confirm that $S_T(MTD)$ = 0.84 > $S_T(e)$ = 0.67 > $S_T(Speed)$ = 0.51, indicating that pavement texture contributes most strongly to the total variance in $F^*_{\max}$, while speed and superelevation have secondary but consistent effects.

(ii) Morris screening (Morris, 1991):

$$\mu_i^* = mean\ (|EE_i|)\,,\ \sigma_i = std(|EE_i|) \tag{24}$$

where EE_i are elementary effects from randomized trajectories.

Table 4. Sobol indices

Parameter	S_{T_i}
MTD	0.839672
Speed	0.511073
e	0.672759

Morris screening (Table 5) further supports this trend: the ranking μ_i^*(MTD) > μ_i^*(Speed) ≫ μ_i^*(e) highlights texture as the most influential factor, with superelevation showing minimal impact.

Table 5. Morris Indices

Parameter	Mean (μ_i^*)	Standard deviation (σ_i)
MTD	0.332865	0.172659
Speed	0.294931	0.151806
e	0.020894	0.010989

Hence, the models are well-conditioned, with sensitivity concentrated in physically meaningful parameters, ensuring that the predicted friction behavior remains stable and interpretable under realistic operating conditions.

6. Validation and comparative evaluation of F_{MAX} models

6.1 Validation against AASHTO and international models

The model ($F^*_{\max}$) was compared with AASHTO (2018) and other international standards,

including South Africa (CSIR, 2000; Austroads, 2021), Sri Lanka (RDA, 1998), Malaysia (REAM, 2002), Abu Dhabi (ADQCC, 2023), Korea (KOTI, 2013; Malawi Roads Authority, 2020), and IRC (2023) (Figure 6). However, AASHTO was used as a benchmark because it provides a well-established speed-dependent friction envelope. In contrast, the IRC standard adopts a constant friction value (0.15) independent of speed or surface texture. Therefore, AASHTO provides a suitable comparative framework for validating the speed-dependent model developed in this study.

The Indian friction model $F^*_{\max}$ Eq. (13), aligns closely with the AASHTO friction envelope at moderate operating speeds (30–60 km/h). At lower speeds (<20 km/h), the model predicts slightly higher friction availability due to the influence of pavement surface texture and superelevation. At higher speeds (>80 km/h), the predicted values remain higher than those suggested by AASHTO, reflecting the influence of mixed-traffic behaviour and pavement heterogeneity typical of Indian highways. This difference arises because the proposed model incorporates field-measured pavement texture (MTD) and local operating speeds, which are not explicitly considered in conventional design guidelines.

Across all models, $F^*_{\max}$ declines consistently with speed (20–140 km/h). For example, AASHTO decreases from 0.36 at 20 km/h to 0.07 at 140 km/h, South Africa from 0.19 at 30 km/h to 0.11 at 120 km/h, and the present study from 0.346 to 0.111. At 60 km/h, the present study predicted 0.183 compared with 0.157 for Malaysia, 0.160 for Sri Lanka, and 0.18 for AASHTO. At 100 km/h, Malaysia and Abu Dhabi estimated 0.115 and 0.12, respectively, while the present study predicted 0.136. Austroads and Korea generally yielded lower values, and Malawi aligned (between 0.11 and 0.14) closely with IRC:73. In contrast, the present study derives friction availability directly from field measurements of pavement texture and operating speeds. Therefore, higher values at lower speeds reflect realistic tire-pavement interaction under Indian roadway conditions. Overall, the present study consistently produced higher friction availability at higher speeds, highlighting the need for region-specific calibration under Indian conditions. This trend reflects the influence of surface texture and road design on safety margins at higher speeds and underscores the need for cautious design at elevated velocities.

In summary, the Present Study aligns with global models at low speeds but predicts higher side friction availability at high speeds compared to AASHTO, Korea, and Austroads. At 140 km/h, the Present Study (0.111) is well above AASHTO (0.07) and close to the conservative IRC:73 (0.15). While adopting conservative standards, such as AASHTO, ensures robust safety margins, the Present Study provides region-specific insights tailored to Indian pavement conditions and mixed-traffic behavior.

6.2 Influence of curve radius

The effect of the curve radius on $F^*_{\max}$ and speed adaptation was examined using both the Indian model and AASHTO data. In the Indian study, distinct patterns emerged: sharp curves (60–80 m radius) were associated with reduced midpoint speeds (V_{middle}) but higher $F^*_{\max}$; Medium-radius curves (100–140 m) showed wide variability in both speed and friction, and flatter curves (>160 m) supported higher speeds with lower friction demand. The scatter within each group reflects heterogeneous driver adaptation strategies in mixed-traffic conditions.

AASHTO results showed similar clustering but with more conservative and uniform friction estimates. At small radii (≈60–80 m, 20–50 km/h), the Indian model predicted $F^*_{\max}$ up to 0.6 compared with AASHTO's 0.4. For medium radii (≈100–140 m, 40–80 km/h), peaks above 0.5 were observed, while AASHTO values remained ≤0.35. Even at large radii (≈160–180 m, 80–100 km/h), the Indian model predicted 0.2–0.3 compared with AASHTO's 0.1–0.2. These results confirm that Indian drivers impose higher friction demands than those assumed in international guidelines.

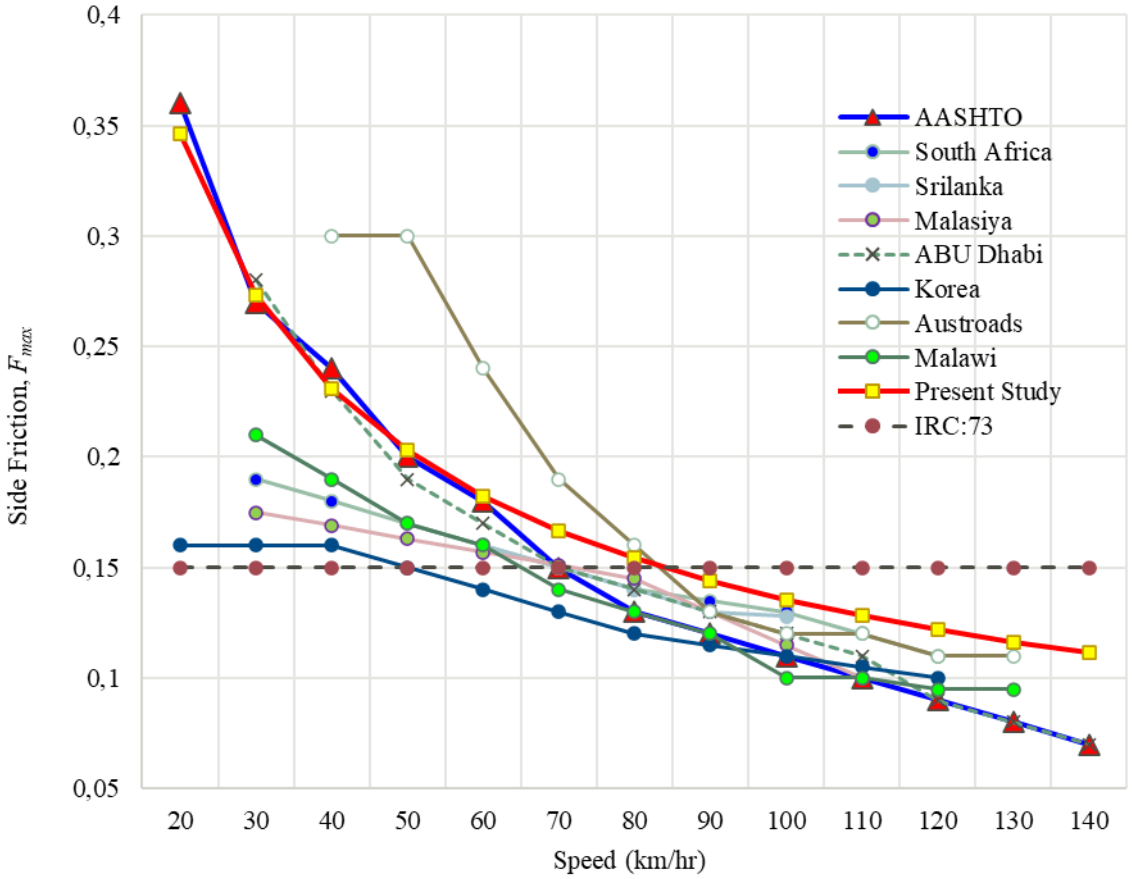

Figure 6. Variation of $F^*_{\max}$ with speed for different models and the present study

Overall, $F^*_{\max}$ declines with increasing speed, with the curve radius significantly influencing the speed–friction relationship. Region-specific calibration is therefore vital, as global models tend to underestimate friction demand under Indian conditions, affecting reliable safety evaluation and design interventions.

7. The safety indices

After developing the F_{max} model specific to the measured field conditions and speed profiles of vehicles under mixed traffic-flow conditions, the safety conditions at three different segments of each curve at start, middle, and end locations were evaluated by using the following three safety indices:

The safety index (SI) is defined as:

$$SI = \frac{F^*_{\max}}{F_d} \tag{25}$$

The above index represents the immediate safety margin between available and required friction. SI values >1.0 indicate safe operating conditions with surplus friction, SI = 1.0 denotes a critical threshold with no margin of safety, and SI<1.0 indicates unsafe operation with a risk of instability (Donnell et al., 2016).

To capture how safety evolves along the curve, the change in safety index **(ΔSI)** was introduced. The variation from:

Approach to midpoint:

$$(\Delta SI_1 = SI_{middle} - SI_{approach}) \tag{26}$$

Midpoint to exit:

$$(\Delta SI_2 = SI_{exit} - SI_{middle}) \tag{27}$$

The above two indices distinguish deteriorating conditions ($\Delta SI < 0$) from improving conditions (ΔSI>0). Negative values indicate heightened risk zones, typically at entry or middle points, while positive values reflect recovery at exits.

The dynamic curve safety index (DCSI) is defined as the ratio:

$$DCSI = \left(\frac{\Delta SI_1}{\Delta SI_2}\right) = \left(\frac{a_1}{a_2}\right) = \frac{\left(V_{middle}^2 - V_{approach}^2\right)}{\left(V_{exit}^2 - V_{middle}^2\right)} \quad (28)$$

The relationship quantifies curve risk balance values near 1.0 denote stability, > 1.0 indicate entry instability, and < 1.0 signal exit instability, while negative DCSI marks critical deceleration–acceleration patterns. Together, SI, ΔSI, and DCSI provide an integrated tool for assessing, tracking, and managing curve safety by combining analysis of speed, texture, and geometry.

8. Curve safety evaluation using safety indices

Curve safety was assessed by linking operating speeds at approach, midpoint, and exit to side-friction demand and supply, and synthesizing these into three indicators: the Safety Index (SI), the Change in Safety Index (ΔSI), and the Dynamic Curve Safety Index (DCSI). Vehicle-class midpoint speeds formed the basis for estimating friction demand, which was compared with the calibrated $F_{\max}^*$ model (Eq. (13)) to compute the indices.

8.1 Safety index (SI)

The SI expresses the balance between available friction ($F_{\max}^*$) and imposed demand (f_d) (Figure 7). Trucks and buses showed the greatest stability, with 76–80% of cases classified as safe (SI > 1.0). Two-wheelers performed even better, with 94.3% of cases safe despite their lower speeds. By contrast, cars showed mixed performance, with 52.3% unsafe, while three-wheelers were the most vulnerable, with 56.9% unsafe at midpoints. These results emphasize vehicle-class disparities: heavy vehicles and two-wheelers were relatively stable due to their lower operating speeds, resulting in lower friction demand, whereas cars often operated near critical friction limits, underscoring the need for targeted speed management. Three-wheelers exhibit higher instability due to their asymmetric three-wheel configuration, narrow wheelbase, and elevated center of gravity, which reduces lateral stability during curve negotiation. In contrast, two-wheelers generally operate at lower speeds and riders tend to adopt conservative maneuvering strategies, resulting in lower friction demand.

8.2 SI variation with radius and speed

SI trends with curve radius reveal that a small radius (≈60–80 m) yielded highly scattered results in the Indian model, while AASHTO predicted predominantly unsafe or near-zero SI. At medium radii (≈100–140 m), Indian outcomes remained widely spread, reflecting heterogeneous driver behavior, whereas AASHTO values were more uniform. At large radii (≈160–180 m), the Indian model stabilized SI in the positive range (≈0.2–0.4) but with higher scatter, while AASHTO produced tightly clustered values (≈0.2–0.3). Thus, the Indian model better reflects mixed-traffic variability, whereas AASHTO offers more conservative, uniform estimates.

8.3 Change in safety index (ΔSI)

ΔSI highlights safety progression along curves. Cars and two-wheelers largely remained in moderate risk (0 < ΔSI < 1), with 12–15% in high risk (ΔSI < 0). Three-wheelers showed marked deterioration, with 17% unsafe at midpoints (ΔSI_1 < 0) and nearly 48% unsafe at exits (ΔSI_2 < 0). Trucks and buses performed well initially, with 59% safe from approach to midpoint (ΔSI_1 > 1), but 46% deteriorated to unsafe conditions at exits (ΔSI_2 < 0). Overall, safety tended to decline from midpoint to exit, with three-wheelers and heavy vehicles most affected.

8.4 Dynamic curve safety index (DCSI)

DCSI assesses captures entry–exit imbalances (Figure 8). Most vehicles fell into moderate risk (DCSI < 1.0), but a large proportion faced high risk (DCSI < 0), including all cars (n = 193) and all two-wheelers (n = 35). Severe instability (DCSI <-1 to <- 3) was particularly evident among three-wheelers and heavy vehicles. Compared with SI and ΔSI, DCSI more strongly revealed exit-segment deficits,

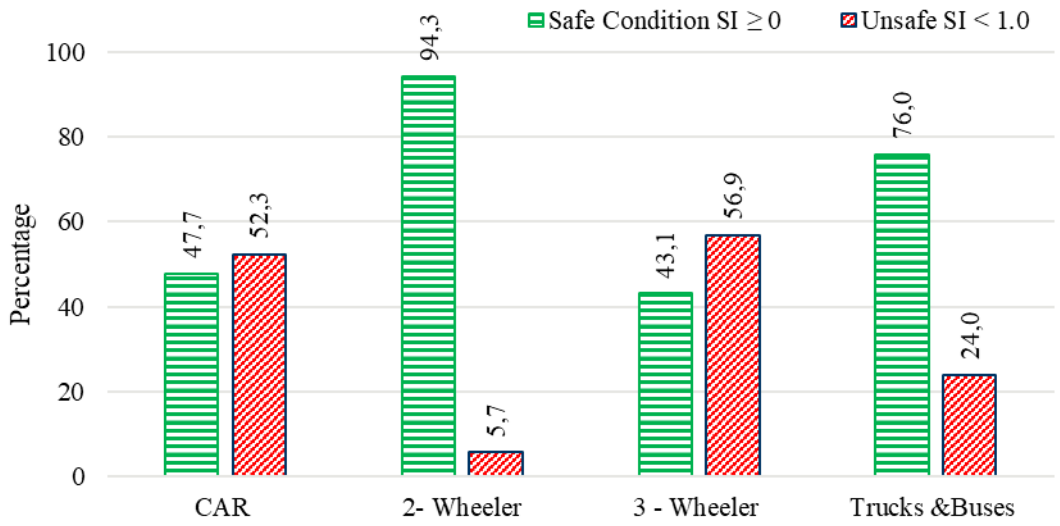

Figure 7. Risk condition vehicles in percent observed based on SI Values

where recovery from midpoint deceleration was insufficient.

Together, SI, ΔSI, and DCSI form a comprehensive diagnostic framework: SI evaluates local stability, ΔSI captures its variation along the curve, and DCSI detects entry-exit imbalances. Integrating operating speed, friction, texture, and geometry, this framework effectively identifies hazardous curves and supports targeted safety interventions such as speed management, alignment correction, and pavement treatment.

9. Results and discussion

Vehicle Speed Profiles: Spot speed surveys on five horizontal curves of NH-340C revealed marked differences across vehicle classes. Cars averaged 79.1 km/h at tangents and 61.4 km/h at midpoints, while three-wheelers were the slowest (≈24.6 km/h). Speed variability was highest for cars (SD: 16.9–18.0 km/h) and lowest for three-wheelers (7.6–8.4 km/h), reflecting heterogeneous driving behavior. Acceleration analysis showed sharp entry decelerations (up to −6.3 m/s^2 for cars), sustained negative accelerations at midpoints, and partial recovery at exits (+0.5 to +1.2 m/s^2). These patterns indicate cautious entry, controlled mid-curve maneuvering, and incomplete exit recovery.

Validation of F_{max} and International Comparisons: The Indian $F^*_{\max}$ model, derived from midpoint speeds, Mean Texture Depth (MTD), and superelevation, closely matched AASHTO trends at moderate speeds (30–60 km/h) but predicted higher values at low (<20 km/h) and high (>80 km/h) speeds, reflecting local pavement and mixed-traffic conditions (Figure 1). At low speeds (<20 km/h), friction demand becomes negligible compared with available friction. Consequently, safety indices remain well above the critical threshold (SI>1), resulting in limited differentiation between models. The proposed framework, therefore, provides greater analytical sensitivity at moderate and high operating speeds where friction demand approaches available limits. Comparisons with international models (South Africa, Austroads, Sri Lanka, Malaysia, Abu Dhabi, Korea, Malawi, and IRC) showed that the present study generally yields higher friction availability at higher speeds, highlighting the need for region-specific calibration (Figure 6).

Influence of Curve Radius on Speed and Friction: Curve radius strongly influenced both $F^*_{\max}$ and operating speeds. The Indian model showed scattered SI and $F^*_{\max}$ values

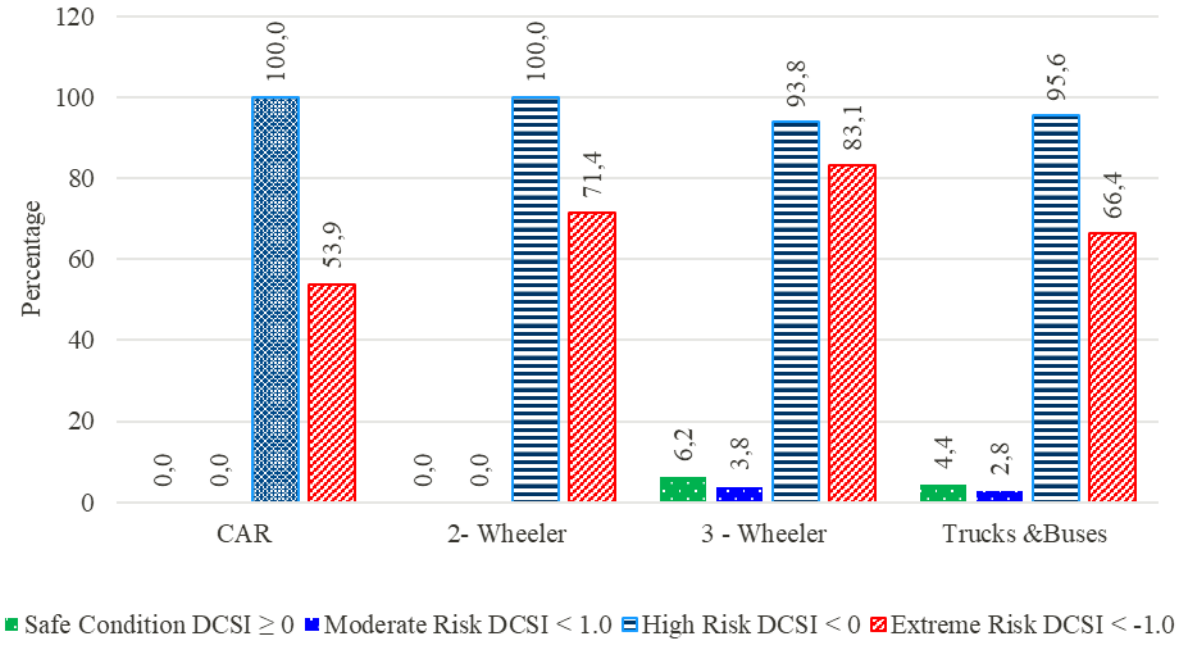

Figure 8. Risk condition vehicles in percent observed based on DCSI values

at small radii (≈60–80 m), wide variability at medium radii (≈100–140 m), and partial stabilization at large radii (>160 m) (Figures 6 and 7). In contrast, AASHTO produced more conservative and tightly clustered predictions (Figure 6). Small-radius curves required F_{max} up to 0.6 under Indian conditions, exceeding the AASHTO limit of 0.4, while medium- and large-radius curves also showed higher and more variable friction demands. These results indicate that Indian drivers impose greater friction demands than international guidelines assume.

Curve Safety Assessment Using SI, ΔSI, and DCSI: Safety evaluation highlighted distinct class-specific patterns (Figures 7 and 8). SI indicated that trucks and buses were largely safe (76–80%), two-wheelers were highly stable (94.3%), while cars and three-wheelers often operated near critical limits (52.3% and 56.9% unsafe, respectively). ΔSI showed deteriorating safety toward exits, especially for three-wheelers ($\Delta SI_1 < 0$ for 23 cases, $\Delta SI_2 < 0$ for 113) and heavy vehicles ($\Delta SI_2 < 0$ for 229). DCSI revealed entry–exit imbalances, with all cars and two-wheelers in high-risk zones (DCSI < 0) and severe instability among three-wheelers and heavy vehicles. Collectively, these indices form a comprehensive framework that integrates speed, friction, pavement texture, and geometry to identify hazardous curves and guide targeted interventions.

Implications for Highway Safety: The analysis demonstrates three critical points: (i) side friction demand decreases as speed increases, (ii) curve radius strongly moderates the speed–friction relationship, and (iii) international models often underestimate friction requirements under Indian conditions. Adoption of a region-specific model of F^*_{max} improves the accuracy of safety assessments and supports interventions such as speed regulation, curve realignment, and pavement treatments, thereby enhancing safety in mixed-traffic environments.

Generalizability of the proposed model: Although the present study uses five curves from NH-340C, the selected curves cover a broad range of geometric and pavement conditions typical of Indian rural highways. The observed radii range between 50 m and 180 m, superelevation between 4 and 7%, and Mean Texture Depth between 0.38 and 1.12 mm. These ranges represent typical design

parameters recommended in IRC standards for two-lane rural highways. Therefore, the calibrated friction model reflects realistic operating conditions under heterogeneous traffic environments. Future research will extend the dataset to multiple highways across different climatic regions of India.

10. Speed prediction model

Field-observed speed profiles reveal a consistent deceleration trend from the curve approach to its midpoint, followed by partial acceleration toward the exit. The mid-curve represents the most critical control point, where three-wheelers record the lowest operating speeds. At the same time, cars exhibit greater variability and more abrupt acceleration patterns, leading to higher differential speeds among vehicle classes. Such fluctuations highlight the necessity of real-time driver advisory systems to maintain safe, uniform speed behavior on horizontal curves.

To quantify these dynamics, a regression-based model was developed to predict mid-curve operating speeds (V_{middle}) under field conditions, using measured approach speeds (V_{start}) and geometric parameters. The calibrated model demonstrates a strong linear relationship, expressed as:

$$V_{middle} = 0.9821\ V_{start} - 4.271 \quad (29)$$

Predicted and observed speeds showed close agreement (Figure 9). From training results, the statistical metrics found as Mean Absolute Percentage Error (MAPE) = 2.72%, Root Mean Square Error (RMSE) = 1.37 km/h, and Coefficient of Determination (R^2) = 0.975, while testing results yielded MAPE = 2.96%, RMSE = 1.68 km/h, and R^2 = 0.962. These metrics confirm the model's reliability and minimal error across datasets.

These results confirm that the model accurately captures the link between approach and midpoint speeds, making it suitable for real-time curve-speed estimation. Trained with field data, it can generate safe speed alerts to improve vehicle stability and reduce excessive friction demand. Such models support safety measures such as dynamic speed display signs (Monsere et al., 2005) and audible warnings (Xu et al., 2023), helping drivers adjust their behavior and reducing crash risk

11. Proposed application

Advisory speed plaques are widely used for curve safety management (Traffic, 2009). Past studies linked advisory speeds to factors such as curve radius, geometry, side friction, superelevation, and warning signs (Bonneson et al., 2007; Dixon & Rohani, 2008; Montella & Imbriani, 2015; Pratt et al., 2019). However, static advisory speeds often prove inadequate due to inconsistent design, varying driver behavior, and differences in decision-making (Nicholson, 1998; Soole et al., 2013). Recent approaches emphasize adaptive systems that monitor real-time speeds and provide automated warnings through visual or audio feedback (Davis et al., 2018; Mahmud et al., 2023).

The safety indices (SI, ΔSI, DCSI) proposed in this study offer a foundation for dynamic curve monitoring. Speed data, obtained via roadside sensors or GPS, can be used to calculate SI and identify unsafe conditions. Risk alerts may then be issued through vehicle-actuated flashing beacons, adaptive electronic signage, or integrated ADAS systems (Antony & Whenish, 2021). This approach supports immediate feedback, particularly under adverse conditions, and allows adjustments by vehicle type and site-specific characteristics.

11.1 Practical application and feasibility of the proposed warning system

The conceptual framework is illustrated in Figures 10 and 11. Approach speed data are collected, side friction demand is estimated, and predicted midpoint speeds (Eq. 29) are applied to compute SI. If SI < 1.0, the system triggers a speed reduction warning. Advisory speeds are dynamically calculated using Eq. (30), which incorporates friction demand, superelevation, curve radius, and gravitational effects to define safe operating

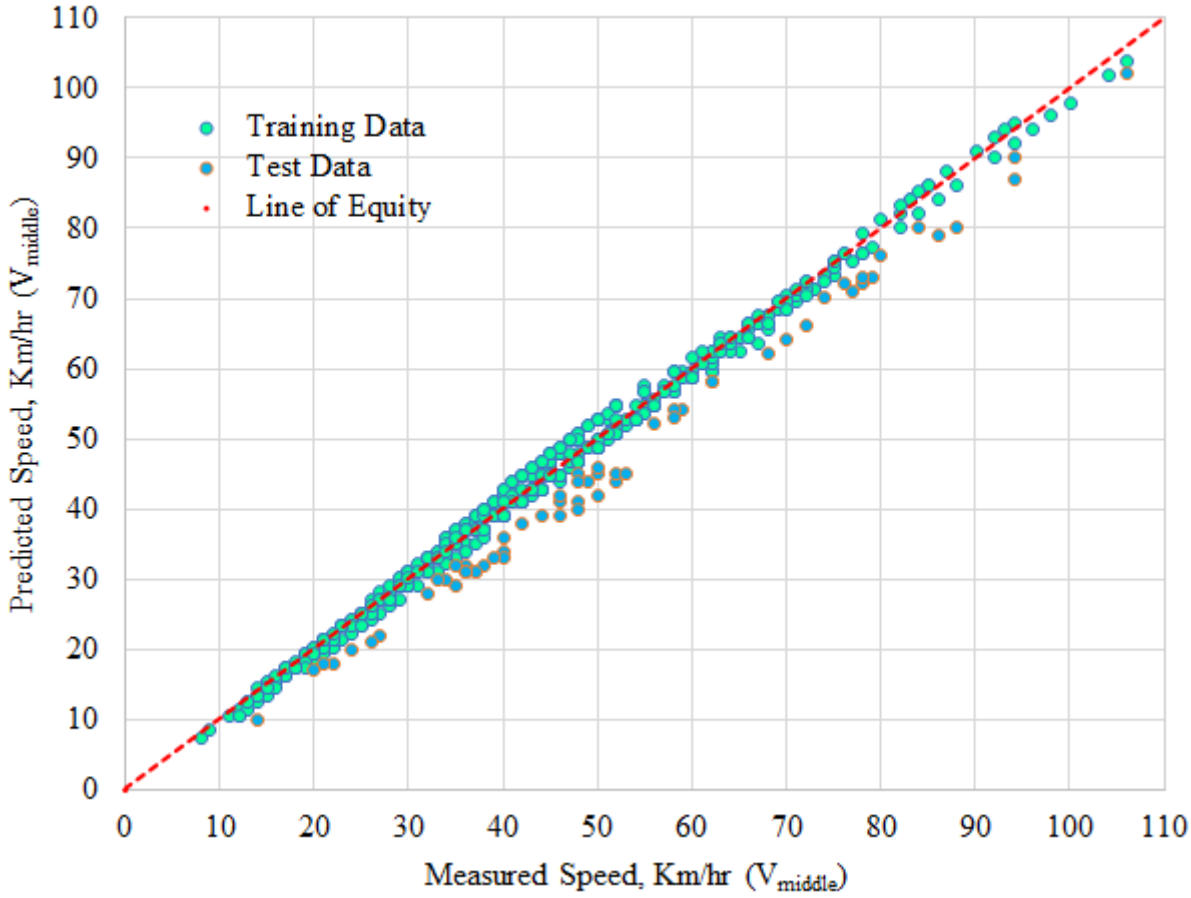

Figure 9. Predicted and measured mid-curve speeds (V_{middle}) using the regression model

limits.

$$V_{advisory} = \sqrt{\frac{gR\,(f_{dmiddle} \times SI + \sin\theta)}{\cos\theta}} \quad (30)$$

Where the term (f_{dmiddle}×SI) represents F^{*}_{max} reflecting the actual friction demand at the predicted speed and the associated risky margin (SI); θ denotes the maximum superelevation, g is the acceleration due to gravity, and R is the curve radius.

Drivers are alerted in real time through flashing beacons, adaptive signs, or in-vehicle notifications. By continuously updating safe speed thresholds along curve segments, the system ensures proactive interventions, reduces friction-related risks, and enhances safety in mixed-traffic environments.

12. Conclusions

This study developed a field-based framework for evaluating horizontal curve safety by integrating measured traffic speeds, pavement surface characteristics, and probabilistic reliability analysis. The framework was applied to five horizontal curves located along NH-340C to examine the relationship between operating speeds, pavement texture, and available side friction. The major findings are summarized as follows:

1. A locally calibrated model for estimating maximum available side friction (Fmax) was developed using field measurements of vehicle speed, Mean Texture Depth (MTD), and superelevation from the study curves. The predicted friction values ranged from 0.16 to 0.28 and showed reasonable agreement with established international guidelines

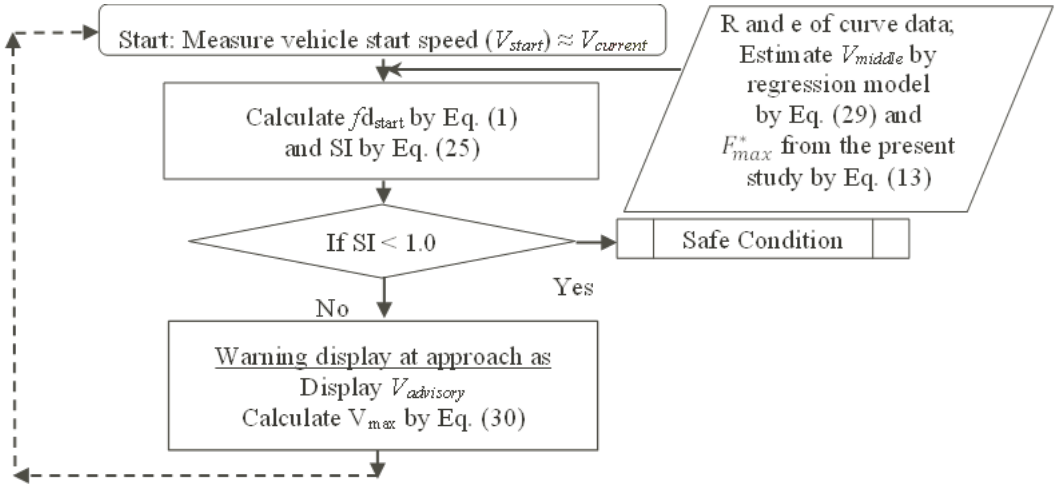

Figure 10. Control logic framework for applying safety index criteria on circular horizontal curves

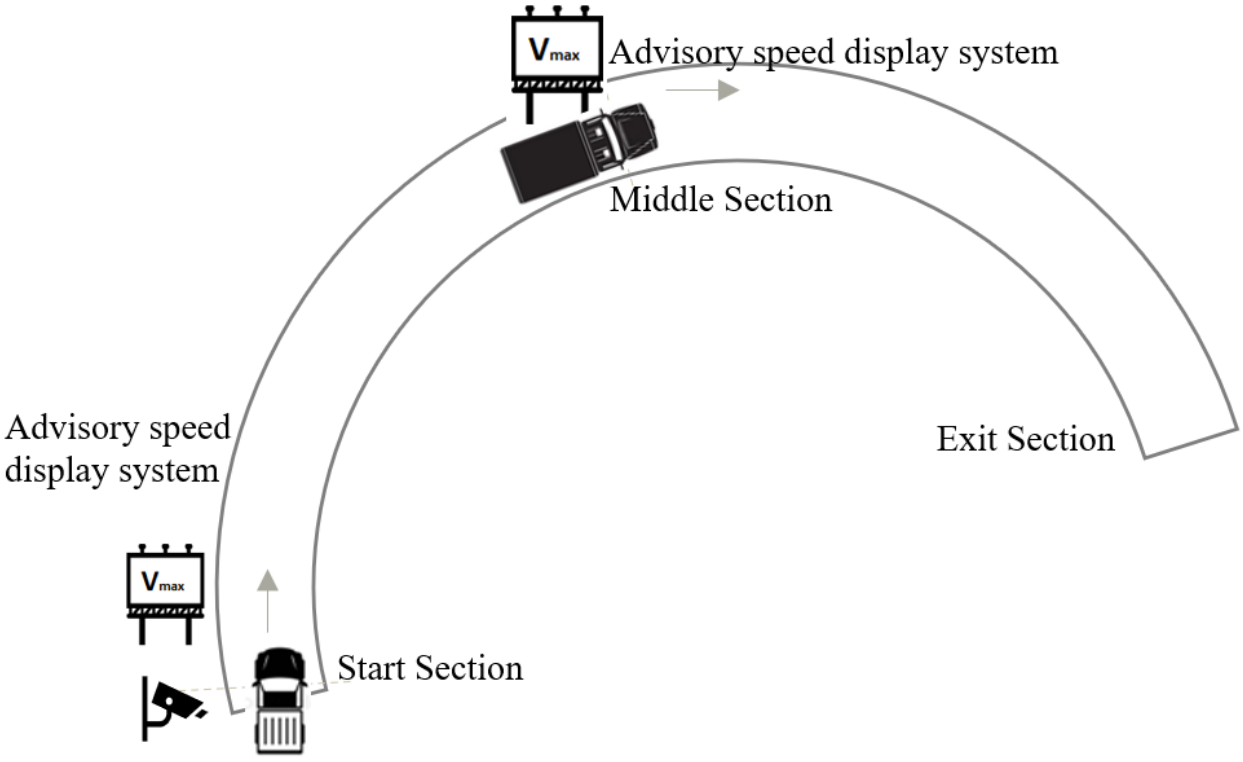

Figure 11. Conceptual framework for implementation $V_{advisory}$ on horizontal curves

while reflecting the observed pavement and mixed-traffic conditions at the selected sites.

2. Uncertainty analysis using the Delta method, bootstrap resampling, and First-Order Reliability Method (FORM) indicated that the calibrated friction model remains statistically stable and provides consistent safety margins across the observed operating speed range.

3. Global sensitivity analysis based on Sobol and Morris methods showed that pavement texture (MTD) has the strongest influence on friction variability, followed by operating speed, while superelevation contributes comparatively less to the variation in available friction.

4. The safety indices provided a useful means of assessing safety conditions along the studied curves. The results suggest that cars and three-wheelers often operate closer to critical friction limits, whereas trucks, buses, and two-wheelers generally exhibit greater stability due to their lower operating speeds.

5. A regression-based speed prediction model was developed to estimate mid-curve operating speeds with good accuracy. The model shows potential for supporting advisory speed estimation and safety monitoring on curves with similar geometric and traffic characteristics.

Overall, the results demonstrate that integrating friction modelling, safety indices, and speed prediction provides a useful analytical approach for evaluating curve safety at the site level and may support future development of adaptive warning systems.

13. Limitations and future work

This study presents a field-based framework for assessing horizontal curve safety by relating vehicle operating speeds, pavement texture, and available side friction. However, several limitations should be acknowledged. The analysis was based on observations from five horizontal curves located along NH-340C. Although the selected curves represent a range of geometric and pavement conditions typical of rural highways, the limited number of study sites restricts the extent to which the results can be generalized beyond the investigated corridor. In addition, all field measurements were conducted under dry pavement conditions in order to isolate the influence of geometry and surface texture on friction availability.

In real-world conditions, environmental factors such as rainfall, pavement wetness, and drainage characteristics can significantly affect tire-pavement interaction and reduce available friction levels. Future studies should therefore incorporate weather-related variables, including rainfall intensity and pavement surface moisture, possibly through continuous monitoring systems or sensor-based measurements. Expanding the dataset to include additional curves from other highway corridors and varying traffic compositions would also improve the robustness and broader applicability of the proposed framework. Further work may also investigate the integration of real-time traffic data and intelligent transportation technologies to support dynamic speed advisory systems for hazardous curves.

CRediT contribution

R. Srinivasa Kumar: Conceptualization, Methodology, Software, Supervision, Writing – original draft, Writing – review & editing. **Vemula Rajesh Kumar:** Data curation, Formal analysis, Investigation.

Acknowledgements

The authors are thankful to the Department of Civil Engineering for continuous support and the Traffic Police Department for permission and assistance during field data collection.

Declaration of competing interests

The authors have no conflicts of interest with other entities or researchers.

Declaration of generative AI use

The authors declare that no generative AI or AI-assisted tools were used in the preparation of this manuscript.

Ethics statement

The research reported in this paper involved field observations of vehicle speeds and roadway characteristics on public highways. No personal or identifiable data were collected from individuals. Therefore, the study did not involve human subjects and did not require formal ethical approval.

Funding statement

No agency was involved in funding this study.

Data availability statement

Data is available upon request.

Editorial information

Handling editor: **Jiří Ambros**, Transport Research Centre (CDV), Czechia.

Reviewer: **Alyssa Ryan**, Michigan State University, the United States of America.

Submitted: 13 March 2026; Accepted: 2 June 2026; Published: 13 June 2026.

References

AASHTO (2018). 'A policy on geometric design of highways and streets'. in . Washington, DC: American Association of State Highway and Transportation Officials.

Abohassan, A., El-Basyouny, K., Kwon, T. J. (2022). 'Effects of inclement weather events on road surface conditions and traffic safety: An event-based empirical analysis framework'. *Transportation Research Record*, 2676, 51–62. 10.1177/03611981221088588

ADQCC (2023). 'TR-514 road design standards'. Technical report, Abu Dhabi Quality and Conformity Council.

Antony, M. M., Whenish, R. (2021). 'Advanced driver assistance systems (ADAS)'. in M. Kathiresh & R. Neelaveni (eds), *Automotive embedded systems* pp. 165–181. Springer.

Austroads (2021). 'Guide to road design part 3: Geometric design (Edition 3.4)'.

Barnett, J. (1938). 'Transition curves for highways'. in . Washington, DC: U.S. Government Printing Office.

Bennett, C. R. (1994). 'A speed prediction model for rural two-lane highways'.

Beutner, E. (2024). 'Delta method: Asymptotic distribution'. *Wiley Interdisciplinary Reviews: Computational Statistics*, 16(1), e1634. 10.1002/wics.1634

Bonneson, J. A. (1999). 'Side friction and speed as controls for horizontal curve design'. *Journal of Transportation Engineering*, 125(6), 473–480. 10.1061/(ASCE)0733-947X(1999)125:6(473)

Bonneson, J. A. (2000). 'Kinematic approach to horizontal curve transition design'. *Transportation Research Record*, 1737, 1–8. 10.3141/1737-01

Bonneson, J. A., Pratt, M. P. (2009). 'Model for predicting speed along horizontal curves on two-lane highways'. *Transportation Research Record*, 2092, 19–27. 10.3141/2092-03

Chen, S. S., Rakotonirainy, A., Loke, S., Krishnaswamy, S. (2007). 'A crash risk assessment model for road curves'. *Proceedings of the 20th International Technical Conference on Enhanced Safety of Vehicles*.

Chen, Z., Fan, W. (2021). 'A freeway travel time prediction method based on an XGBoost model'. *Sustainability*, 13(15), 8577.

CSIR (2000). 'Guidelines for human settlement planning and design: Roads—Geometric design and layout planning'.

Dash, D. P., Sethi, N., Dash, A. K. (2020). 'Identifying the causes of road traffic accidents in India: An empirical investigation'. *Journal of Public Affairs*, 20, e2038. 10.1002/pa.2038

Davis, B., Morris, N. L., Achtemeier, J. D., Patzer, B. (2018). 'In-vehicle dynamic curve-speed warnings at high-risk rural curves'.

Dixon, K., Rohani, J. (2008). 'Methodologies for estimating advisory curve speeds on Oregon highways'. Technical report, Oregon Department of Transportation.

Donnell, E., Wood, J., Himes, S., Torbic, D. (2016). 'Use of side friction in horizontal curve design: A margin of safety assessment'. *Transportation Research Record*, 2588, 61–70. 10.3141/2588-07

Figueroa Medina, A. M., Tarko, A. P. (2007). 'Speed changes in the vicinity of horizontal curves on two-lane rural roads'. *Journal of Transportation Engineering*, 133(4), 215–222. 10.1061/(ASCE)0733-947X(2007)133:4(215)

Fitzpatrick, K., ... (2000). 'Design factors that affect driver speed on suburban arterials'. Technical report, Texas Transportation Institute.

Fleiter, J., Watson, B. (2005). 'The speed paradox: The misalignment between driver attitudes and speeding behaviour'. *Australasian Road Safety Research, Policing and Education Conference*.

Gattis, J. L., Vinson, B. F., Duncan, L. K. (2005). 'Low-speed horizontal curve friction factors'. *Journal of Transportation Engineering*, 131(2), 112–119. 10.1061/(ASCE)0733-947X(2005)131:2(112)

Gong, H., Stamatiadis, N. (2008). 'Operating speed prediction models for horizontal curves on rural four-lane highways'. *Transportation Research Record*, 2075, 1–7. 10.3141/2075-01

Han, L., Du, Z., Zheng, H., Xu, F., Mei, J. (2023). 'Reviews and prospects of human factors research on curve driving'. *Journal of Traffic and Transportation Engineering*.

Hassen, A., Godesso, A., Abebe, L., Girma, E. (2011). 'Risky driving behaviours for road traffic accidents among drivers in Mekele city, Northern Ethiopia'. *BMC Research Notes*, 4, 535.

Himes, S., Porter, R. J., Hamilton, I., Donnell, E. (2019). 'Safety evaluation of geometric design criteria: Horizontal curve radius and side friction demand on rural two-lane highways'. *Transportation Research Record*, 2673, 516–525.

Hummer, J. E., Rasdorf, W. J., Findley, D., Zegeer, C. V. (2010). 'Procedure for curve warning signing, delineation, and advisory speeds for horizontal curves'. Technical report, North Carolina Department of Transportation.

IRC (2023). 'IRC:73-2023 geometric design standards for non-urban roads'. Technical report, Indian Roads Congress.

KOTI (2013). 'Ten lessons from road transport policy in Korea'. Technical report, Korea

Transport Institute.
Lee, E. H. (2023). 'Traffic speed prediction of urban road network based on high-importance links using XGBoost and SHAP'. *IEEE Access*.
Levenberg, K. (1944). 'A method for the solution of certain nonlinear problems in least squares'. *Quarterly of Applied Mathematics*, 2(2), 164–168.
Llopis-Castelló, D., González-Hernández, B., Pérez-Zuriaga, A. M., García, A. (2018). 'Speed prediction models for trucks on horizontal curves of two-lane rural roads'. *Transportation Research Record*, 2672, 72–82.
Lu, X., Chen, C., Gao, R., Xing, Z. (2023). 'Prediction of high-speed traffic flow around cities based on a BO-XGBoost model'. *Symmetry*, 15(7), 1453.
Mahmud, M. S., Bamney, A., Megat Johari, M. U., Jashami, H., Gates, T. J., Savolainen, P. T. (2023). 'Evaluating driver response to a dynamic speed feedback sign at rural highway curves'. *Transportation Research Record*, 2677, 1103–1114.
Malawi Roads Authority (2020). 'Low volume roads manual: Geometric design and road safety'.
Marquardt, D. W. (1963). 'An algorithm for least-squares estimation of nonlinear parameters'. *SIAM Journal on Applied Mathematics*, 11(2), 431–441.
McLean, J. (1981). 'Driver speed behaviour and rural road alignment design'. *Traffic Engineering and Control*, 22.
Melchers, R. E., Beck, A. T. (2018). 'Structural reliability analysis and prediction'. in . Wiley.
Milstead, R., Qin, X., Katz, B., Bonneson, J. A., Pratt, M., Miles, J., Carlson, P. J. (2011). 'Procedures for setting advisory speeds on curves'. Technical report, Federal Highway Administration.
Montella, A., Imbriani, L. L. (2015). 'Safety performance functions incorporating design consistency variables'. *Accident Analysis & Prevention*, 74, 133–144.
Morris, M. D. (1991). 'Factorial sampling plans for preliminary computational experiments'. *Technometrics*, 33(2), 161–174.
MoRTH (2022). 'Road accidents in India 2022'. Technical report, Ministry of Road Transport and Highways, Government of India.
MoRTH (2023). 'Annual report 2023–24'. Technical report, Ministry of Road Transport and Highways, Government of India.
MoRTH (2024). 'Annual report 2024–25'. Technical report, Ministry of Road Transport and Highways, Government of India.
Nicholson, A. (1998). 'Superelevation, side friction, and roadway consistency'. *Journal of Transportation Engineering*, 124(5), 411–418.
Parsa, A. B., Movahedi, A., Taghipour, H., Derrible, S., Mohammadian, A. K. (2020). 'Toward safer highways: Application of XGBoost and SHAP for real-time accident detection'. *Accident Analysis & Prevention*, 136, 105405.
Pratt, M. P., Geedipally, S. R., Pike, A. M. (2015). 'Analysis of vehicle speeds and speed differentials in curves'. *Transportation Research Record*, 2486, 28–36.
Saltelli, A., Annoni, P., Azzini, I., Campolongo, F., Ratto, M., Tarantola, S. (2010). 'Variance-based sensitivity analysis of model output'. *Computer Physics Communications*, 181(2), 259–270.
Semeida, A. M. (2014). 'Application of artificial neural networks for operating speed prediction at horizontal curves'. *Journal of Modern Transportation*, 22, 20–29.
Shalkamy, A., Gargoum, S., El-Basyouny, K. (2021). 'Towards a more inclusive and safe design of horizontal curves'. *Accident Analysis & Prevention*, 153, 106009.
Singh, S. K. (2017). 'Road traffic accidents in India: Issues and challenges'. *Transportation Research Procedia*, 25, 4708–4719.
Sobol, I. M. (2001). 'Global sensitivity indices for nonlinear mathematical models and their Monte Carlo estimates'. *Mathematics and Computers in Simulation*, 55, 271–280.
WHO (2023). 'World health statistics 2023: Monitoring health for the SDGs'. Technical report, World Health Organization.
Yang, Y., Wang, K., Yuan, Z., Liu, D. (2022). 'Predicting freeway traffic crash severity using an XGBoost-Bayesian network model'. *Journal of Advanced Transportation*.
Zhao, C., Zhao, X., Li, Z., Zhang, Q. (2022). 'XGBoost-DNN mixed model for predicting driver behaviour during lane-changing decisions'. *Sustainability*, 14, 6829.
Zhou, W., Gong, C., Hong, H. P. (2017). 'New perspective on application of first-order reliability method for estimating system reliability'. *Journal of Engineering Mechanics*, 143(9).